JOURNAL of the MEXICAN CHEMICAL SOCIETY

https://www.jmcs.org.mx/

Article

Open Access

J. Mex. Chem. Soc. **2026**, *70(1):e2572*

Received October 10th, 2025
Accepted February 9th, 2026

http://dx.doi.org/10.29356/jmcs.v70i1.2572
e-location ID: 2572

Keywords:
[3+2] cycloaddition reaction; electron localization function; molecular electron density theory; bond evolution theory; non-covalent interactions.

Palabras clave:
Reacción de cicloadición [3+2]; función de localización electrónica; teoría de la densidad electrónica molecular; teoría de la evolución del enlace; interacciones no covalentes.

***Corresponding author:**
Ali Ben Ahmed
email: ali.benahmed@isbs.usf.tn

ISSN-e 2594-0317

Mapping Reactivity and Stereochemical Evolution of Benzothiazolium Salts in [3+2] Cycloadditions Using Molecular Electron Density Theory

Mohamed Chellegui[1,2], Raghad Mowafak Al-Mokhtar[4], Raad Nasrullah Salih[4], Lakhdar Benhamed[5], Sofiane Benmetir[6,7], Jesus Vicente de Julián-Ortiz[6], Haydar A. Mohammad-Salim[8,9], Ali Ben Ahmed[10,11*]

[1]Laboratory of Organic Chemistry (LR17ES08), Faculty of Sciences, University of Sfax, 3038 Sfax, Tunisia.
[2]Namur Institute of Structured Matter, University of Namur, Rue de Bruxelles, 61, B-5000 Namur, Belgium.
[3]Department of Chemistry, College of Science, University of Duhok, Duhok 42001, Kurdistan Region, Iraq.
[4]Nursing Department, Bardarash Technical Institute, Akre University for Applied Science, Duhok 42001, Kurdistan Region, Iraq.
[5]Laboratory of Applied Thermodynamics and Molecular Modelling (LAT2M), Department of Chemistry, Faculty of Science, University of Tlemcen, PB 119, Tlemcen, 13000, Algeria.
[6]Department of Physical Chemistry, Faculty of Pharmacy, University of Valencia, Av. Vicente Andrés Estellés s/n, 46100 Valencia, Spain.
[7]Process and Environmental Engineering Laboratory (LIPE), Faculty of Chemistry, University of Science and Technology of Oran Mohamed BOUDIAF, P.O. Box 1503, El Mnaouer, 31000 Oran, Algeria.
[8]Department of Chemistry, Faculty of Science, University of Zakho, Zakho 42002, Kurdistan Region, Iraq.
[9]TCCG Lab, Scientific Research Center, University of Zakho, Zakho 42002, Kurdistan Region, Iraq.
[10]Department of Biomedical, Higher Institute of Biotechnology of Sfax, University of Sfax, BP 1175 - 3000 Sfax-Tunisia.
[11]Laboratory of Applied Physics, Department of Physics, Faculty of Sciences, University of Sfax, BP 1171 - 3000 Sfax-Tunisia.

J. Mex. Chem. Soc. **2026**, *70(1):e2572*
Regular Issue

ISSN-e 2594-0317

Abstract. The electronic structure of the benzothiazolium salt 1 (1-(cyanomethyl)-2,3-dihydro-1H-benzothiazol-1-ium) and its reactivity in [3+2] cycloaddition (32CA) reactions with dimethyl(Z)-2-butenedioate 2 have been investigated using Molecular Electron Density Theory (MEDT) combined with Density Functional Theory (DFT) calculations at the M06-2X/6-311+G(d,p) level. Topological analysis of the Electron Localization Function (ELF) reveals that 1 act as a carbenoid-type three-atom component (TAC), characterized by a carbenoid C3 center. Conceptual DFT reactivity indices identify this TAC as a moderate electrophile and a supernucleophile. The polar 32CA reaction proceeds via a one-step asynchronous mechanism, as revealed by the Bond Evolution Theory (BET), and involves the formation of two stable molecular complexes. The activation barriers are low for both the endo and exo pathways. DFT calculations indicate that the endo pathway is slightly both kinetically and thermodynamically preferred over the exo one, in agreement with experimental findings. Non-covalent interactions (NCIs) analysis attributes this endo selectivity to a combination of weaker attractive interactions and enhanced van der Waals and repulsive interactions in TS-endo, which alleviates steric strain and stabilizes the TS.

Resumen. La estructura electrónica de la sal de benzotiazolio 1 (1-(cianometil)-2,3-dihidro-1H-benzotiazol-1-io) y su reactividad en reacciones de cicloadición [3+2] (32CA) con el dimetil (Z)-2-butendioato 2 se investigaron utilizando la Teoría de la Densidad Electrónica Molecular (MEDT) en combinación con cálculos de la Teoría del Funcional de la Densidad (DFT) al nivel M06-2X/6-311+G(d,p). El análisis topológico de la Función de Localización Electrónica (ELF) revela que el compuesto 1 actúa como un componente de tres átomos (TAC) de tipo carbenoide, caracterizado por un centro carbenoide C3. Los índices de reactividad de la DFT conceptual identifican a este TAC como un electrófilo moderado y un supernucleófilo. La reacción polar de cicloadición 32CA transcurre mediante un mecanismo asincrónico de una sola etapa, tal como lo revela la Teoría de la Evolución del Enlace (BET), e implica la formación de dos complejos moleculares estables. Las barreras de activación son bajas tanto para las vías endo como exo. Los cálculos DFT indican que la vía endo está ligeramente favorecida, tanto desde el punto de vista cinético como termodinámico, con respecto a la vía exo, en concordancia con los resultados experimentales. El análisis de las interacciones no covalentes (NCI) atribuye esta selectividad endo a una combinación de interacciones atractivas más débiles y de interacciones de van der Waals y repulsivas más intensas en el estado de transición TS-endo, lo que reduce la tensión estérica y estabiliza dicho estado de transición.

Introduction

A three-atom component (TAC) can react with an acetylene derivative through a [3+2] cycloaddition (32CA) process, widely recognized as one of the most efficient synthetic approaches for constructing five-membered heterocyclic compounds. This reaction is especially remarkable for its capacity to produce cyclic products with excellent regio- and stereoselectivity in organic synthesis [1]. Among TACs, benzothiazolium salt **1** plays a prominent role and is commonly used in 32CA reactions. It has the potential to yield pharmacologically active isoxazolidines and isoxazolines, which are well-defined in terms of both regio- and stereochemistry [2].

Density functional theory (DFT) has played a key role in understanding 32CA reactions involving TACs. Computational studies have demonstrated that DFT reliably predicts regio- and stereoselectivity, in good agreement with experimental findings [2,3]. The classification of TACs and acetylene derivatives according to the absolute electrophilicity scale has further clarified the influence of electronic effects on the cycloaddition process [4]. Moreover, mechanistic investigations have revealed that these reactions can proceed through polar pathways, either via a concerted or a stepwise mechanism, particularly in systems involving benzothiazolium salt **1** [5,6]. A significant advancement came in 2016 when Domingo introduced the Molecular Electron Density Theory (MEDT), which emphasizes the role of electron density variations in governing the reactivity of organic processes [7].

MEDT has since become a foundational framework for understanding molecular reactivity in organic chemistry [8–10] highlighting electron density changes as the principal driving force behind reaction behavior.

http://dx.doi.org/10.29356/jmcs.v70i1.2572

J. Mex. Chem. Soc. **2026**, *70(1):e2572*
Regular Issue

ISSN-e 2594-0317

MEDT-based studies have revealed that numerous 32CA reactions follow a non-concerted one-step mechanism characterized by sequential bond formation, distinguishing them from the concerted pericyclic pathways proposed by Woodward and Hoffmann in 1969. Although many 32CA reactions are inherently non-polar, the regioselectivity observed in polar variants can be effectively rationalized through Parr function analysis [11,12]. Tang and co-workers conducted DFT studies on the reactivity of 1,3-dialkynes with ammonia derivatives, providing valuable insights into the reaction mechanisms [13,14]. Subsequent theoretical investigations revealed that these 32CA reactions generally proceed through a single-step mechanism with asynchronous bond formation, rather than through a fully concerted pathway [13,15,16]. Overall, 32CA reactions exhibit a wide range of reactivity patterns. *Pseudodiradical* (*pdr*)-type 32CA reactions, which possess relatively low activation energies, generally occur more easily [16,17]. In contrast, *zwitterionic* (*zw*)-type 32CA reactions are associated with higher energy barriers and depend more strongly on the electrophilic-nucleophilic interactions between the reactants to proceed [18].

Within the framework of MEDT, various quantum chemical tools have been effectively utilized to investigate the reactivity, selectivity, and mechanistic features of cycloaddition reactions. Conceptual DFT (CDFT) provides both global and local reactivity descriptors that enable a rationalization of the electronic structure of the reactants and prediction of their chemical behavior [19–24]. To refine this analysis, Parr functions are employed to pinpoint the most nucleophilic and electrophilic regions in the reacting species, thereby offering valuable insight into regioselectivity trends [11,12]. To further characterize bonding interactions, Quantum Theory of Atoms in Molecules (QTAIM) [25], based on Bader's quantum theory, is applied to examine the topology of the electron density, allowing for the identification of bond critical points and the quantification of intra- and intermolecular interactions [26,27]. In parallel, the Electron Localization Function (ELF) [28] is used to visualize electron pairing and localization in real space, distinguishing bonding regions, lone pairs, and core electron domains. To complement the analysis of covalent interactions, Non-Covalent Interaction (NCI) [29] analysis is employed to identify and visualize weak intermolecular forces such as hydrogen bonding, dispersion, and steric effects through the topology of the electron density and its reduced density gradient. These interactions, though subtle, play a significant role in stabilizing transition state structure (TS) and shaping stereoselectivity [3,30]. Finally, the Bonding Evolution Theory (BET) [31–34] provides a dynamic perspective by analyzing the continuous changes in electron density along the intrinsic reaction coordinate (IRC) [35], particularly in the vicinity of bifurcation points, offering a detailed understanding of bond formation and cleavage during the course of the reaction [36,37].

In this investigation, MEDT is employed to elucidate the reaction mechanism and the stereoselectivity of the 32CA reaction between benzothiazolium salt **1** (1-(cyanomethyl)-2,3-dihydro-1H-benzothiazol-1-ium) and dimethyl(Z)-2-butenedioate **2** (Scheme 1) [38]. This reaction was originally reported by Kraus et al. and carried out in acetonitrile at 0 °C, affording the corresponding cycloadduct **3** (2-cyano-3-(2,3-dihydro-1H-benzothiazol-1-yl)-1,2,3,6-tetrahydroiso- indole-1,3-dicarboxylate) in 89% yield. Notably, the reaction proceeds with a marked *endo* stereoselectivity (Scheme 1). Thus, using BET, this work focuses on the reaction mechanism by showing a) how and where the formation/breakage of bonds take place, b) how the electron density is distributed and reorganized, c) whether this reaction occurs following a concerted mechanism or not, while addressing its (a)synchronicity, d) to propose a reaction mechanism for this reaction. To further clarify the factors governing reactivity and selectivity, the analysis is complemented by NCI, QTAIM, and ELF studies, resulting in a comprehensive understanding of the electronic and structural elements that control the stereoselectivity observed experimentally.

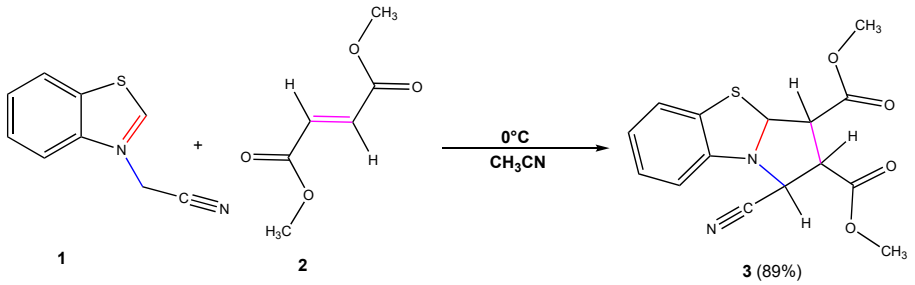

Scheme 1. 32CA reaction between benzothiazolium salt **1** and dimethyl(Z)-2-butenedioate **2**

http://dx.doi.org/10.29356/jmcs.v70i1.2572

J. Mex. Chem. Soc. **2026**, *70(1):e2572*
Regular Issue

ISSN-e 2594-0317

Computational methods

TThe geometries of all chemical species were optimized using the M06-2X exchange-correlation functional [39] and the 6-311+G(d,p) basis set. This level of theory has been demonstrated to be reliable for studying this type of reaction [40,41]. Stationary points were confirmed as true minima by the absence of imaginary frequencies, while TSs were verified by the presence of a single imaginary frequency. Departing from each TS, calculations were performed to describe the structures and energies along the IRC [35]. Solvent [acetonitrile, ε = 35.94] effects were modeled with the IEFPCM (*integral equation formalism of the polarizable continuum model*) method [42]. Calculations were performed for T = 273.15 K and, initially, for P = 1.0 atm.

To characterize the polarity of the reaction, the global electron density transfer (GEDT) [43] at the TS was computed as the sum of the natural atomic charges (q), obtained by a natural bond orbital (NBO) analysis [44], of the atoms belonging to each framework (f):

$$\mathrm{GEDT} = \sum_{i \in f} q_i \tag{1}$$

Positive values mean an electronic flux from the considered framework to the other one, and *vice versa.* Following the approach of conceptual DFT [21,45], several descriptors of the electronic structure and reactivity were evaluated, employing the energies of the highest occupied molecular orbital (HOMO, ε_H) and the lowest unoccupied molecular orbital (LUMO, ε_L), i.e. the global electrophilicity ($\omega = \mu^2/2\eta$) [46], the chemical potential [$\mu = (\varepsilon_H + \varepsilon_L)/2$] [45], and the global hardness ($\eta = \varepsilon_L - \varepsilon_H$) [47]. The nucleophilicity index (N) is defined as $N = \varepsilon_H$ (Nu) − ε_H (TCE), where Nu is the nucleophile and TCE is the tetracyanoethylene reference [48].

The local indices defined from the Parr, Pearson, and Yang functions [11,12] were determined from natural population analysis (NPA) [44,49] of the neutral species as well as of their radical anions and cations. The atomic spin density (ASD) was adopted to describe these functions, in order to assess the polarity of the reactions. The Parr functions, defined as $P_k^+ = q_k(N+1) - q_k(N)$ for electrophilic attack and $P_k^- = q_k(N) - q_k(N-1)$ for nucleophilic attack, were written in terms of the respective population q_k (N) of k^{th} atomic site of the N-electron system. The local electrophilicity ($\omega_k = \omega \times P_k^+$) [4], and the local nucleophilicity indices ($N_k = N \times P_k^-$) [50], were calculated. For a given reaction, Domingo et al. [51] proposed a local reactivity difference index ($R_k = \omega_k - N_k$), for the determination of the most electrophilic and nucleophilic centers of the species participating in the reaction. All calculations were carried out with the Gaussian16 software package [52].

The NCI [29] analysis was highlighted by performing a single-point calculation on each optimized TS geometry. Then, the corresponding plots of the electron density [ρ(r)] versus the reduced density gradient (RDG) were obtained by using the NCIPLOT program [53]:

$$\left[\boldsymbol{s(r)} = \left| \frac{\boldsymbol{\nabla_\rho(r)}}{\boldsymbol{2(3\pi^2)^{1/3}\rho(r)^{4/3}}} \right| \right] \tag{2}$$

To evaluate the nature of the bonding properties of the forming/breaking bonds that take place along the reaction pathways, a QTAIM analysis was first carried out using the Multiwfn program [54]. Then, to decipher the formation of these bonds along the reaction coordinate, a BET analysis was carried out by extracting the wavefunction at each point of the IRCs. The ELFs analysis was performed by means of the TopMod package [55] considering a grid step of 0.2 bohr. Finally, the ELF basin positions and populations were visualized using the DrawMol and DrawProfile programs [56,57].

http://dx.doi.org/10.29356/jmcs.v70i1.2572

J. Mex. Chem. Soc. **2026**, *70(1):e2572*
Regular Issue

ISSN-e 2594-0317

Results and discussion

ELF and NPA characterizations of reagents

To predict the reactivity of the two reagents in this 32CA reaction, an ELF topological analysis was first performed to characterize the electronic structure of the reactants, to establish a correlation between their electronic structure and reactivity [58,59]. The basin attractor positions and populations of the most significant valence basins are shown in Fig. 1.

The ELF topological analysis of the TAC **1** shows the presence of one monosynaptic basins, V(C3), integrating a total electron density of 1.20e, two disynaptic basins, V(C1,N2) and V(C3,N2), with a total electron population of 3.31e and 2.02e, respectively. These ELF basins are related with the presence of a C3 *carbenoid* center, a C1-N2 double bond and an C3-N2 single bond. The presence of a monosynaptic basin at the C3 carbon integrating higher than 1.0e, which are associated with a *carbenoid* C3 center, allows the classification of the TAC **1** as a *carbenoid* TAC [60] participating in *carbenoid-type* (*cb-type*) 32CA reactions [61]. The ELF of **2** shows the presence of two disynaptic basins,V(C4,C5) and V'(C4,C5), integrating a total population of 3.33e, associated with a C4-C5 double bond.

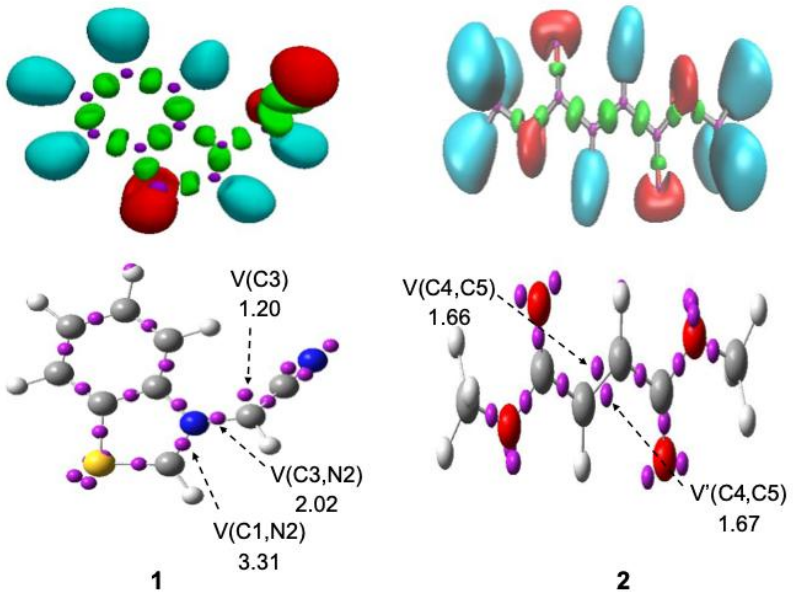

Fig. 1. IEFPCM(acetonitrile)/M06-2X/6–311+G(d,p) ELF basin attractor positions (isosurface, η = 0.75) and the most significant ELF valence basin populations of the reactants **1** and **2**.

The charge distribution of **1** and **2** was analyzed through NPA (see Scheme 2). In TAC **1**, the N2 nitrogen and the C3 carbon atoms are highly negatively charged by -0.31e, and -0.43e, respectively, while the C1 carbon atom shows a low negative charge of -0.08e. As shown in Scheme S1, the N2 nitrogen atom carries a positive charge according to QTAIM and Mulliken analyses, consistent with the Lewis-like representation of a salt. The NPA of **2** shows negative charges of -0.23e at both C4 and C5 carbon atoms. Basing on ELF analysis and NPA charge distribution, the proposed Lewis-like structures of reagents are given in Scheme 2.

http://dx.doi.org/10.29356/jmcs.v70i1.2572

J. Mex. Chem. Soc. **2026**, *70(1):e2572*
Regular Issue

ISSN-e 2594-0317

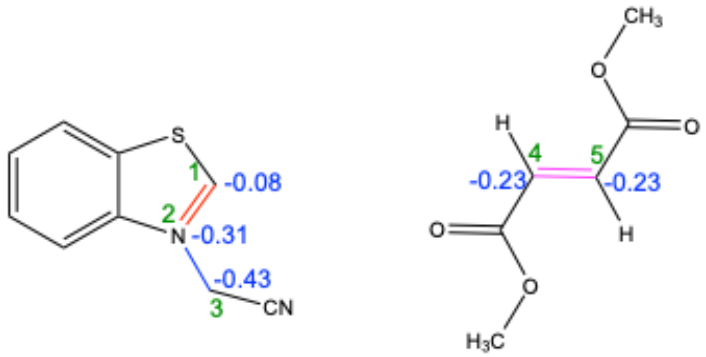

1 **2**

Scheme 2. IEFPCM(acetonitrile)/M06-2X/6–311+G(d,p) Proposed Lewis-like structures together with the natural atomic charges in average number of electrons (in blue color), e, of reactants **1** and **2**.

CDFT analysis

The CDFT descriptors serve as fundamental parameters for assessing the chemical reactivity of compounds involved in cycloaddition reactions [62–68]. The electronic chemical potential of **1** (-3.9 eV) is higher than that of **2** (-5.8 eV) (Table 1), suggesting that the GEDT in this 32CA reaction occurs from **1** to **2**. This observation is also supported by the following findings: (i) the electrophilicity index of **2** (2.0 eV) is greater than that of **1** (1.4 eV), and (ii) the nucleophilicity index of **1** (4.0 eV) is significantly higher than that of **2** (0.5 eV). In addition, according to the electrophilicity and nucleophilicity scales [69], **2** is a strong electrophile (ω = 4.0 eV) and a very low nucleophile (N = 0.5 eV). While **1** (ω = 2.87 eV, N = 4.0 eV) being classified as a moderate electrophile and a strong nucleophile (Table 1). The supernucleophilic character of **1**, N > 4.0 eV, together with the strong electrophilic character of **2**, indicates that the corresponding 32CA reaction will have a high polar character, being classified as of forward electron density flux (FEDF) [70].

Table 1. IEFPCM(acetonitrile)/M06-2X/6–311+G(d,p) Electronic properties (eV).

Reactants	ε_H	ε_L	μ	η	ω	N
1	-6.5	-1.2	-3.9	2.65	2.87	4.0
2	-10.0	-1.6	-5.8	4.2	4.0	0.5

Within a polar 32CA process including asymmetric compounds, the most preferred reaction route is that involving the two-center interaction between the most electrophilic and the most nucleophilic centers of the two reagents [71]. Numerous studies have demonstrated that the electrophilic P_k^+ and nucleophilic P_k^- Parr functions [72], which arise from the excess spin electron density accumulated through the GEDT, rank among the most reliable descriptors for assessing local reactivity in polar and ionic processes [73]. Accordingly, based on the nature of the reactants, the nucleophilic P_k^- Parr functions of **1** and the electrophilic P_k^+ Parr functions of **2** were examined (see Fig. 2).

The two C1 and C3 carbon atoms of **1** are nucleophilically activated by P_k^- = 0.09 and 0.79, respectively, with the C3 carbon being the most nucleophilic center of the TAC. Note that the N2 nitrogen is nucleophilically deactivated (P_k^- = -0.11) (Table S1). On the other hand, the analysis of electrophilic P_k^+ Parr functions at the reactive sites of **2** indicates that the C4 and C5 carbon atoms are both most electrophilic centers, having a value of P_k^+ = 0.26 (Table S1). Therefore, it is predictable that along this 32CA reaction the most favorable nucleophilic/electrophilic interaction will take place with C3 atom of **1** and C4(C5) of **2**.

http://dx.doi.org/10.29356/jmcs.v70i1.2572

J. Mex. Chem. Soc. **2026**, *70(1):e2572*
Regular Issue

ISSN-e 2594-0317

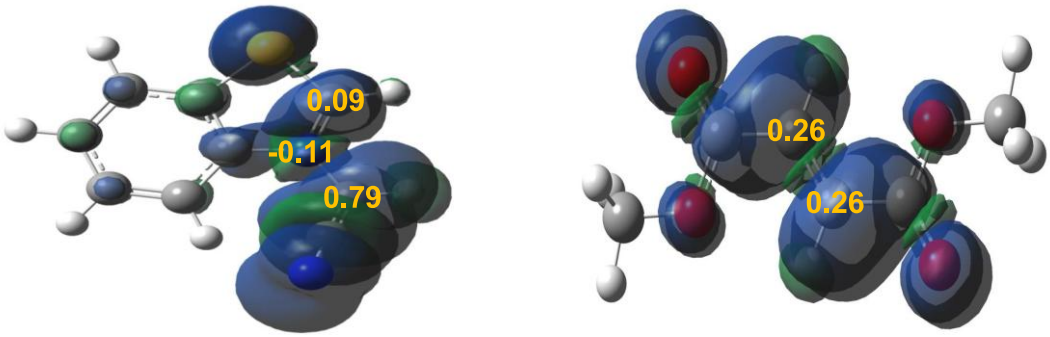

Fig. 2. IEFPCM(acetonitrile)/M06-2X/6–311+G(d,p) Three-dimensional (3D) representations of the atomic spin densities (ASD) (η = 0.02) of the radical cation $1^{\cdot+}$ and the radical anion $2^{\cdot-}$, together with the nucleophilic P_k^- Parr functions of **1** and the electrophilic P_k^+ Parr functions of **2**.

Analysis of the potential energy surfaces for the studied 32CA reaction

Due to the non-symmetry of two reagents **1** and **2**, this 32CA reaction can take place through two stereoisomeric channels, the *endo* and the *exo* (see Scheme 3), i.e., those associated with the initial formation of the C1–C5(C4) and C3–C4(C5) single bonds, respectively. A search for the stationary points involved in the two stereoisomeric pathways allowed finding two molecular complexes (MCs), **MC**-*endo* (**MCN**) and **MC**-*exo* (**MCX**), two stereoisomeric TSs, **TS**-*endo* (**TSN**) and **TS**-*exo* (**TSX**), and the corresponding cycloadducts (CAs), **CA**-*endo* (**CN**) and **CA**-*exo* (**CX**), (see Scheme 3). The total and relative energies of the stationary points associated with the 32CA reaction between **1** and **2** are presented in Tables 2 and S2, respectively, while the corresponding activation energy profile is illustrated in Fig. 3.

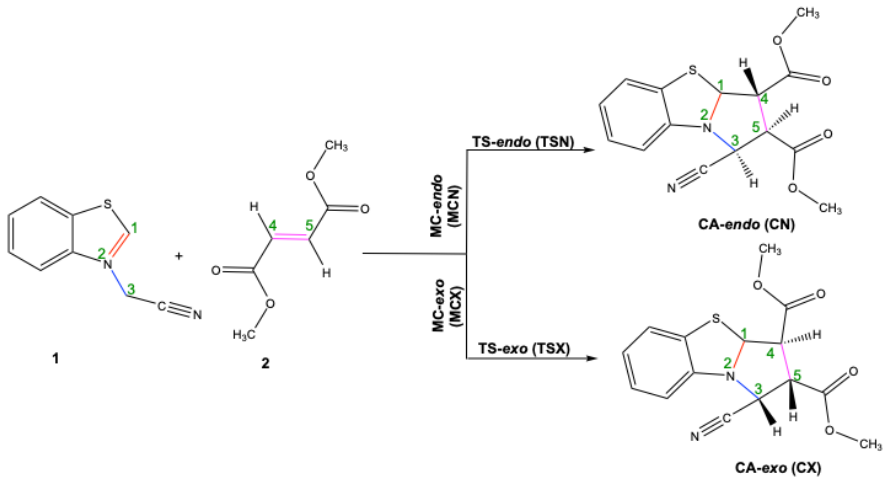

Scheme 3. Competitive reaction paths associated with the 32CA reactions of benzothiazolium salt **1** with dimethyl(Z)-2-butenedioate **2**.

As benzothiazolium salt **1** and dimethyl(Z)-2-butenedioate **2** gradually approach each other, the energy decreases until the formation of two MCs, located 8.97 and 10.96 kcal mol^{-1}, for **MCN** and **MCX**, respectively, below the separated reactants (see Fig. 3). The approach of frameworks **1** and **2** leads to two TSs, **TSN** and **TSX**, lying 1.41 and 3.12 kcal mol^{-1} above **MCN** and **MCX**, respectively, which are in thermodynamic

http://dx.doi.org/10.29356/jmcs.v70i1.2572

J. Mex. Chem. Soc. **2026**, *70(1):e2572*
Regular Issue

ISSN-e 2594-0317

equilibrium. Formation of the **CN** and **CX** cycloadducts is highly exothermic, releasing 48.85 and 51.59 kcal mol^{-1}, respectively. The activation energy difference between **TSN** and **TSX** is ΔΔE = 0.27 kcal mol^{-1} (Fig. 3), within the expected DFT uncertainty (~1 kcal mol^{-1}). The Maxwell-Boltzmann populations [74] show that **TSN** (60.12 %) is slightly more favored than **TSX**, indicating a modest preference for the *endo* path leading to the **CN** cycloadduct (Tables 2 and S2). The strongly exothermic nature of the reaction renders the formation of both **CN** and **CX** products essentially irreversible. To assess the impact of long-range dispersion interactions, additional calculations were performed at the IEFPCM(acetonitrile)/M06-2X-D3/6–311+G(d,p) level of approximation (Tables S4-S6). The results show that dispersion effects lead to a nearly uniform stabilization of all stationary points without altering the relative energetics or the reaction selectivity.

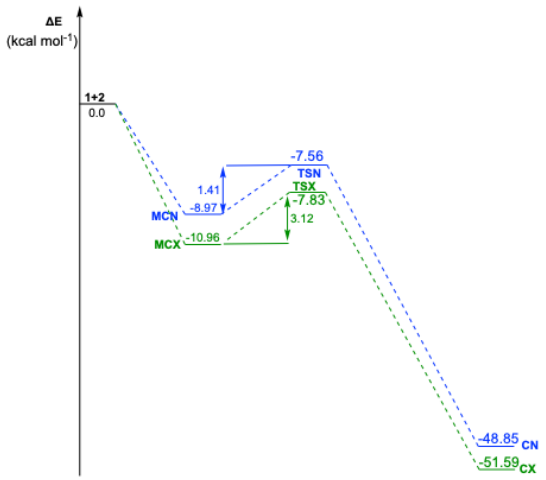

Fig. 3. IEFPCM(acetonitrile)/M06-2X/6–311+G(d,p) Energy profile (ΔE, in kcal mol^{-1}) of the studied 32CA reaction.

Table 2. IEFPCM(acetonitrile)/M06-2X/6–311+G(d,p) Thermochemical state functions (ΔE, ΔH, ΔG, in kcal mol^{-1} and ΔS in cal mol^{-1} K^{-1}), compared to (a) MCN and (b) MCX complexes, of the studied 32CA reaction.

Species	ΔE	ΔH	ΔS	ΔG
TSN	1.41[(a)]	1.08	-9.69	3.97
TSX	3.12[(b)]	2.79	-5.76	4.50
CN	-39.88[(a)]	-37.37	-11.38	-33.97
CX	-40.64[(b)]	-38.18	-8.60	-35.62

Fig. 4 depicts the geometries of the MCs, TSs, and CAs for the 32CA reaction between **1** and **2**. Key parameters [75] including interatomic distances at the reaction centers (r) new bond formation (l), asymmetry index (Δl), and GEDT are reported, with the average electron populations in dimethyl(Z)-2-butenedioate **2** summarized in Table 3.

In the initial stage of the studied 32CA reaction, corresponding to **MCN** and **MCX** formation, both *endo* and *exo* pathways show that the distances between reaction centers C1–C5 and C3–C4 remain outside the typical range for bond formation in a TS. This indicates that no new single bonds are formed in the MCs. Additionally, GEDT values below 0.05e confirm that none of the MCs constitutes an electron density transfer complex (EDTC) [76].

http://dx.doi.org/10.29356/jmcs.v70i1.2572

J. Mex. Chem. Soc. **2026**, *70(1):e2572*
Regular Issue

ISSN-e 2594-0317

The subsequent step in the reaction involves the formation of the TS (Table 3, Fig. 4). In this TS, the C1–C5 and C3–C4 bond distances are notably shorter than the corresponding distances observed in the MC. For the **TSN**, the extent of C1–C5 and C3–C4 forming new bonds is 0.418 and 0.503, respectively. For the **TSX**, the extent of C1–C5 and C3–C4 forming new bonds is 0.343 and 0.531, respectively. These values indicate that for both the **TSN** and **TSX**, the formation of the C3-C4 bond involving the *carbenoid* C3 carbon is more advanced than the C1–C5 bond. For the *endo* and *exo* pathways, the Δl values are 0.085 and 0.188 Å, respectively, which indicates that both TSs exhibit an asynchronous character, with **TSN** being less asynchronous than **TSX**. At both **TSN** and **TSX**, the GEDT presents a very high value, 0.33 and 0.34e, which accounts for their polar character. Therefore, these reactions are classified as FEDF reactions, which is in good agreement with the CDFT analysis.

Table 3. IEFPCM(acetonitrile)/M06-2X/6–311+G(d,p) Key parameters of critical structures for the studied 32CA reaction.

Structures	r_{C1-C5} (Å)	l_{C1-C5}	r_{C3-C4} (Å)	l_{C3-C4}	Δl	**GEDT (e)**
MCN	2.935	---	2.801	---	---	0.01
MCX	3.376	---	3.212	---	---	0.03
TSN	2.492	0.418	2.309	0.503	0.085	0.33
TSX	2.560	0.343	2.272	0.531	0.188	0.34
CN	1.575	---	1.542	---	---	---
CX	1.545	---	1.547	---	---	---
$l_{C1-C5} = 1 - \frac{r^{TS}_{C1-C5} - r^{P}_{C1-C5}}{r^{P}_{C1-C5}}$, $l_{C3-C4} = 1 - \frac{r^{TS}_{C3-C4} - r^{P}_{C3-C4}}{r^{P}_{C3-C4}}$, and $\Delta l = \lvert l_{C3-C4} - l_{C1-C5} \rvert$						

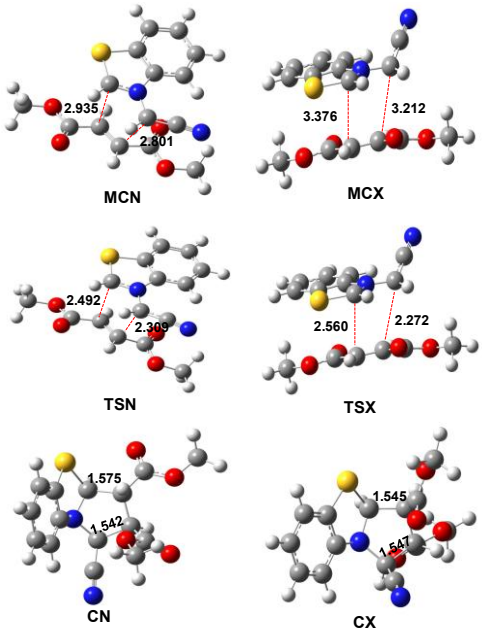

Fig. 4. IEFPCM(acetonitrile)/M06-2X/6–311+G(d,p) Optimized geometries of the key structures (MCs, TSs and CAs) involved in the 32CA reaction between **1** and **2**. The C1–C5 and C3–C4 distances values are given in Å.

http://dx.doi.org/10.29356/jmcs.v70i1.2572

J. Mex. Chem. Soc. **2026**, *70(1):e2572*
Regular Issue

ISSN-e 2594-0317

ELF topological analysis at the TSs

Topological analyses using the ELF were conducted to elucidate the electronic structures of the TSs involved in this 32CA reaction (Fig. 5). The ELF of both **TSN** and **TSX** show the presence of two monosynaptic basins, V(C1) and V(C3), at the benzothiazolium salt **1** framework with a total population of 0.23-0.86e. The electron population in the C1-N2 bonding region diminished from 3.31e at the benzothiazolium salt **1** (Fig. 1) to 3.05e (**TSN**) and 3.12e (**TSN**). The decrease in population indicates the cleavage of the C1-N2 double bond in the TSs, resulting in the emergence of non-bonding electron density on the C1 carbon atom. Furthermore, the population within the disynaptic basin V(C3,N2) increased from 2.02e in **1** to 2.20 e in **TSN** and 2.18e in **TSX**.

On the other hand, the ELF of both **TSN** and **TSX** display the presence of another disynaptic basin, V(C4,C5), at the **2** frameworks with a total electron density value of 3.13e and 3.15e at the **TSN** and **TSX**, respectively. Notably, in both TSs, the absence of a new disynaptic basins, V(C3,C4) and V(C1,C5) indicates that the C-C covalent bond formation had not yet begun.

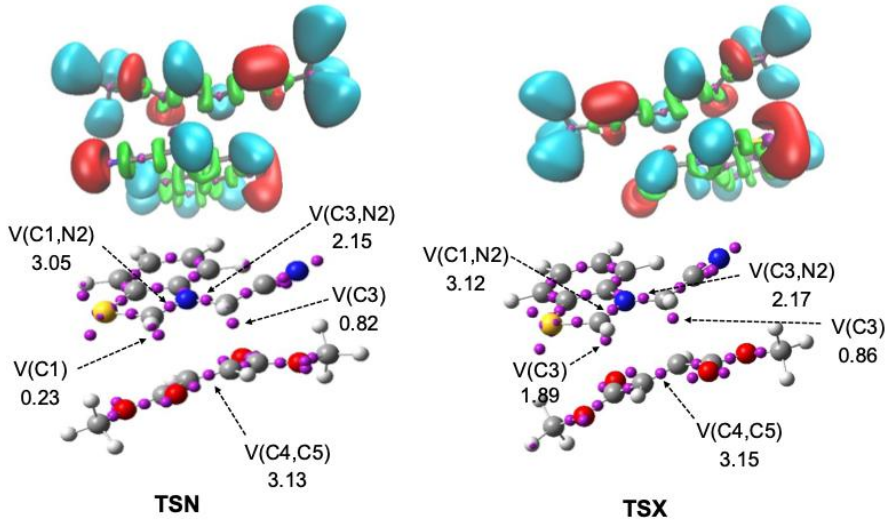

Fig. 5. IEFPCM(acetonitrile)/M06-2X/6–311+G(d,p) ELF basin attractor positions (isosurface, η = 0.75) of the most relevant valence basins of **TSN** and **TSX**.

QAIM analysis of the TSs

TT¿o accurately analyze chemical processes at designated sites, especially during the creation of new carbon-carbon (C-C) bonds, the values of ρ and $\nabla^2\rho$ at the bond critical points (BCPs), labelled as CP1 and CP2, are presented in Table 4. As illustrated in Fig. 6, two nascent BCPs were identified within the TSs: one situated between the C3 and C5, and another between the C4 and C1 atoms.

At both **TSN** and **TSX**, the electron density ρ(r) at these BCPs consistently remained below 0.1 a.u. This observation, coupled with the small, positive values of $\nabla^2\rho(r)$, strongly suggests that the interactions in these nascent bond regions are predominantly non-covalent. Consequently, it can be inferred that the formation of the new C3–C5 and C1–C4 covalent bonds has not yet been fully initiated at these TSs, a conclusion that aligns with the findings from the ELF study (Fig. 5) as well as with the analysis the geometric structures of the TSs (Fig. 4). Furthermore, for both the *endo* and *exo* TSs of the 32CA reaction between **1** and **2**, the ρ(r) values at the C1–C4 BCP (ranging from 0.049 to 0.053 a.u.) were slightly higher than those at the C3–C5 BCP (ranging from 0.030 to 0.034 a.u.). This disparity in electron density at the forming bond regions further emphasizes the inherent asynchronicity of the bond formation process. The consistent presence of positive $\nabla^2\rho(r)$ values at each BCP additionally supports the conclusion regarding the nascent or incomplete nature of the new covalent bonds.

http://dx.doi.org/10.29356/jmcs.v70i1.2572

J. Mex. Chem. Soc. **2026**, *70(1):e2572*
Regular Issue

ISSN-e 2594-0317

Table 4. IEFPCM(acetonitrile)/M06-2X/6–311+G(d,p) QTAIM parameters, the electron density ρ, and the Laplacian of electron density $\nabla^2\rho(r)$, in a.u., of CP1 and CP2 at the TSs associated with the studied 32CA reaction.

Structures	**CP1 (C3-C5)**		**CP2(C1-C4)**	
TSs	**ρ**	**∇^2p (r)**	**ρ**	**∇^2p (r)**
TSN	0.030	0.048	0.053	0.048
TSX	0.034	0.050	0.049	0.050

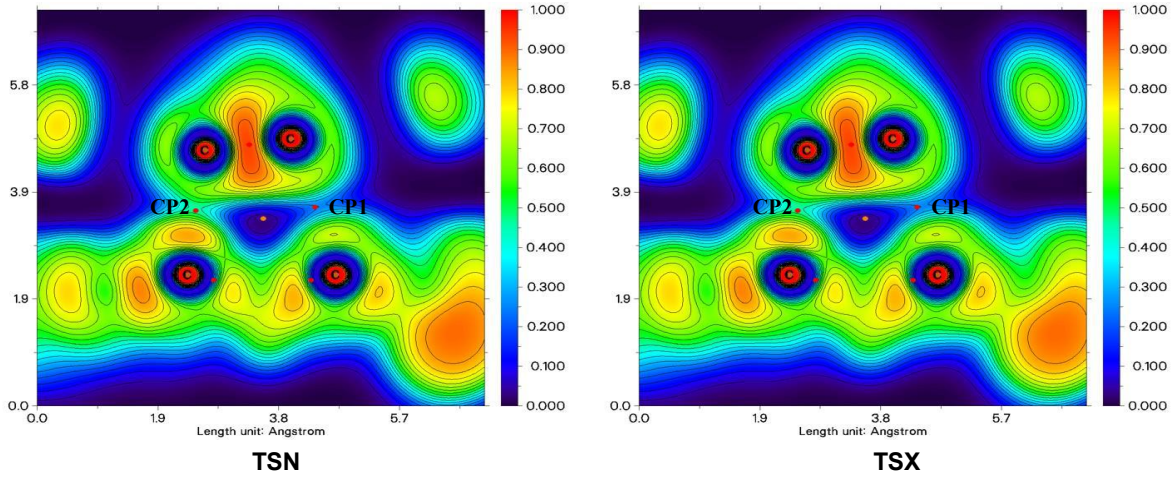

Fig. 6. IEFPCM(acetonitrile)/M06-2X/6–311+G(d,p) Two-dimensional representations of the color-filled maps of the ELF, in the C1-C4 and C3-C5 molecular planes of **TSN** and **TSX**. (3,-1) cps with $\nabla^2\rho_{cp} < 0$ are colored in blue, while cps with $\nabla^2\rho_{cp} > 0$ are colored in red.

NCI analysis of the TSs

The NCI analysis at both **TSN** and **TSX** revealed the presence of non-covalent contacts such as C···H, N···H, and O···H, suggesting the involvement of unconventional hydrogen bonding that may further stabilize these TSs (Fig. 7). The RDG analysis, based on the sign of the second eigenvalue of the Hessian matrix (λ2) and electron density (ρ), reveals that **TSX** exhibits a prominent dark blue region between atoms C1–C4 and C3–C5, indicating strong attractive NCIs. In contrast, **TSN** displays a diminished blue region, with a relative increase in green (van der Waals) and red (repulsive) interactions. The RDG isosurface for **TSN** further confirms significant attractive interactions between C1–C3 and C4–C5, consistent with the lower activation energy observed for **TSN** compared to **TSX**. To further support this conclusion, a quantitative NCI analysis based on the integration of the electron density over the NCI regions was carried out (Figs. 8-10 and Tables S7-8) [77].

http://dx.doi.org/10.29356/jmcs.v70i1.2572

J. Mex. Chem. Soc. **2026**, *70(1):e2572*
Regular Issue

ISSN-e 2594-0317

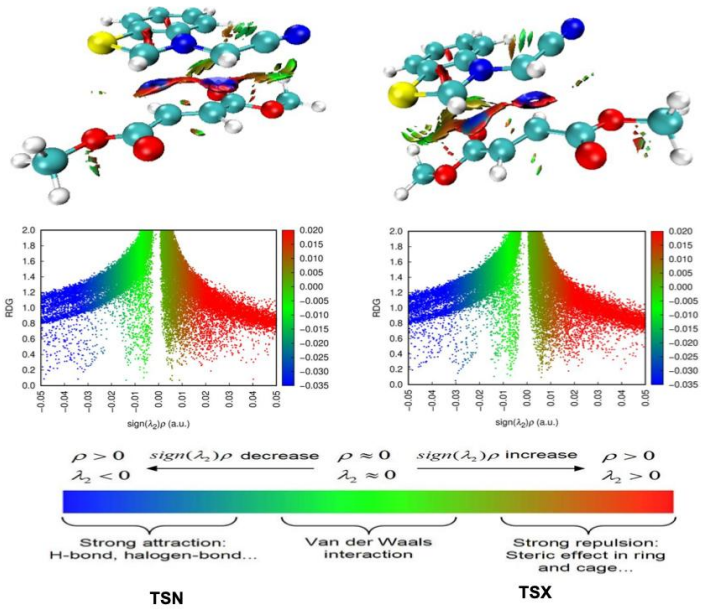

Fig. 7. IEFPCM(acetonitrile)/M06-2X/6–311+G(d,p) NCI and RDG analysis for **TSN** and **TSX** involved in this 32CA reaction. NCI gradient isosurfaces are shown with η = 0.08.

The multilevel grid analysis shown in Figures 8 and 9 reveals clear differences between the two TSs, **TSN** displays a more dispersed distribution of active regions, whereas **TSX** exhibits a pronounced localization of points within the (ρ, s) cutoff domain. As a result, the finest-grid active boxes are more spatially confined for **TSX**, indicating a more localized contribution to the isosurface compared to **TSN**.

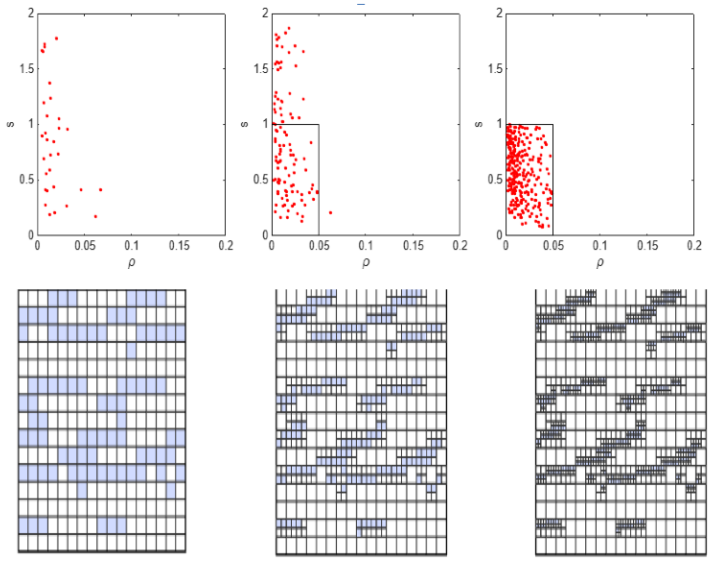

Fig. 8. IEFPCM(acetonitrile)/M06-2X/6–311+G(d,p) Two-dimensional schematic diagram of multilevel grids for **TSN**, from coarse (left) to fine grids (right) with 4:2:1 increment and $\rho_c = 0.05$ and $s_c = 1.0$. The density and the s values are computed at the active points of the coarse, medium, and fine grids (from left to right). Top, cutoff on (ρ,s); bottom, size of the boxes. The small blue boxes are the active boxes of the finest grid, which really contribute to forming the isosurface.

http://dx.doi.org/10.29356/jmcs.v70i1.2572

J. Mex. Chem. Soc. **2026**, *70(1):e2572*
Regular Issue

ISSN-e 2594-0317

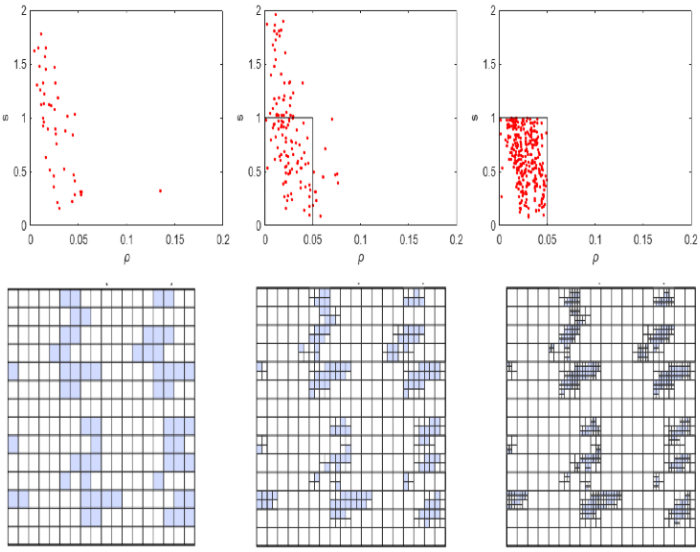

Fig. 9. IEFPCM(acetonitrile)/M06-2X/6–311+G(d,p) Two-dimensional schematic diagram of multilevel grids for **TSX**, from coarse (left) to fine grids (right) with 4:2:1 increments and ρc = 0.05 and sc = 1.0. The density and the s values are computed at the active points of the coarse, medium, and fine grids (from left to right). Top, cutoff on (ρ,s); bottom, size of the boxes. The small blue boxes are the active boxes of the finest grid, which really contribute to forming the isosurface.

Consistently, Fig. 10 shows that under a fixed reduced density gradient cutoff ($s_c = 1.0$) and a stringent density reconstruction parameter ($\gamma_{\text{ref}} = 0.95$), the Ω_{NCI} distributions of both TSs are highly selective and dominated by a limited number of points. While the overall patterns are similar, subtle differences in point density and color distribution point to variations in the extent and strength of the noncovalent interactions. These qualitative observations are fully supported by the quantitative data reported in Tables S7 and S8. **TSN** systematically exhibits larger integrated NCI electron densities and higher density moments at all RDG cutoffs, indicating more extensive and stronger noncovalent interaction regions. In addition, the more pronounced increase of all I_n moments with increasing s_c for **TSN** reflects a broader spatial distribution and a greater weight of NCIs, in contrast to the more localized and weaker interactions characterizing **TSX**.

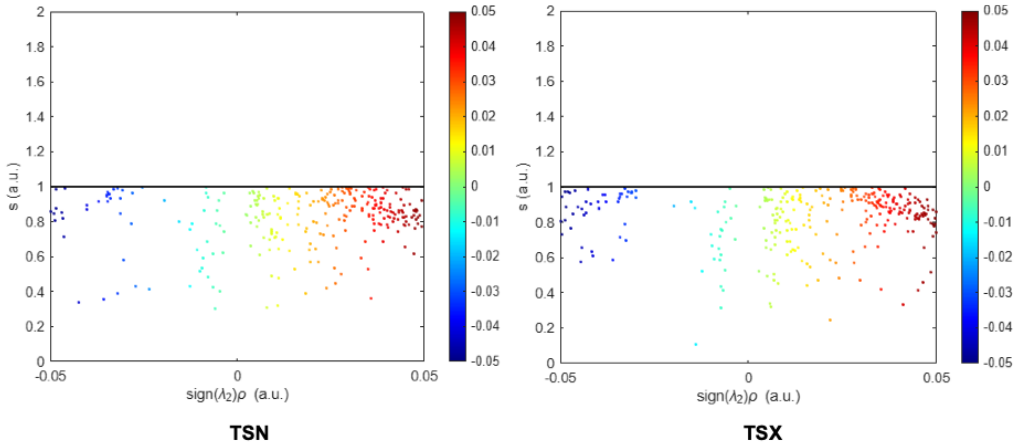

Fig. 10. IEFPCM(acetonitrile)/M06-2X/6–311+G(d,p) Ω_{NCI} defined from the density reconstruction and constant s for **TSN** and **TSX**. Parameters used: $\gamma_{\text{ref}} = 0.95$ (this can be seen from the smaller concentration of points) and $s_c = 1.0$ (black line).

http://dx.doi.org/10.29356/jmcs.v70i1.2572

J. Mex. Chem. Soc. **2026**, *70(1):e2572*
Regular Issue

ISSN-e 2594-0317

BET analysis of the most TSN favorable pathway

The BET analysis of the **TSN** stereoisomeric pathway for the 32CA reaction between compounds **1** and **2** indicates that the reaction proceeds through six distinct structural stability domains (**SSDs**), as depicted in Fig. 11, which illustrates the evolution of the basin populations involved in this process (see Table S9). In **SSD-I** [d(C1−C4) = 2.93 Å and d(C3−C5) = 2.79 Å], the ELF topologies correspond to those of the reactants (Table S9). Compound **1** exhibits one V(C3) monosynaptic basin, integrating 0.69e, associated with the *pseudoradical* center at the C3 carbon, and two disynaptic basins, V(C1,N2) and V(C3,N2), with populations of 2.99e and 2.21e, consistent with the C1−N2 double bond and C3−N2 single bond, respectively. Note that the V(C3) monosynaptic basin integrates less of 1.0e. Compound **2** displays a disynaptic basin corresponding to the C4−C5 double bond, V(C4,C5), with a population of 3.29e.

The transition to **SSD-II** [d(C1−C4) = 2.60 Å and d(C3−C5) = 2.32 Å] is marked by a decrease in the V(C1,N2) basin population due to the emergence of a new monosynaptic basin, V(C1), with a population of 0.10 e, formed via a fold-F type catastrophe. In **SSD-III** [d(C1−C4) = 2.52 Å and d(C3−C5) = 2.22 Å], V(C1,N2) continues to diminish as another monosynaptic basin, V(N2), with a population of 0.56 e, is generated through a fold-F catastrophe. By the end of this domain, the populations of V(C3), V(N2), and V(C1) reach 0.87, 0.65, and 0.19 e, respectively (Fig. 12).

In **SSD-IV** [d(C1−C4) = 2.44 Å and d(C3−C5) = 2.11 Å], the reduction of the V(C4,C5) basin population begins and generates the appearance of another F catastrophe with the creation of the two new monosynaptic V(C4) and V(C5) basins with a total population of 0.20 and 0.17e, respectively (Fig. 11). The two monosynaptic basins V(C3) and V(C5), join together in the **SSD-V** domain [d(C1−C4) = 2.37 Å and d(C3−C5) = 1.99 Å] to form the new V(C3,C5) disynaptic basin holding 1.28e, by the means of a cusp-C type catastrophe, which corresponds to the formation of the C3−C5 single bond. The formation of the V(C1,C4) basin is the last topological change, appearing in the **SSD-VI** domain [d(C1−C4) = 1.92 Å and d(C3−C5) = 1.64 Å] and accounting for the C1-C4 bond formation by means of another C-type catastrophe. At the beginning of **SSD-VI**, the V(C1,C4) basin has a total of 1.52e that are mainly taken from the disappearing of the monosynaptic V(C1) and V(C4) basins (Fig. 12).

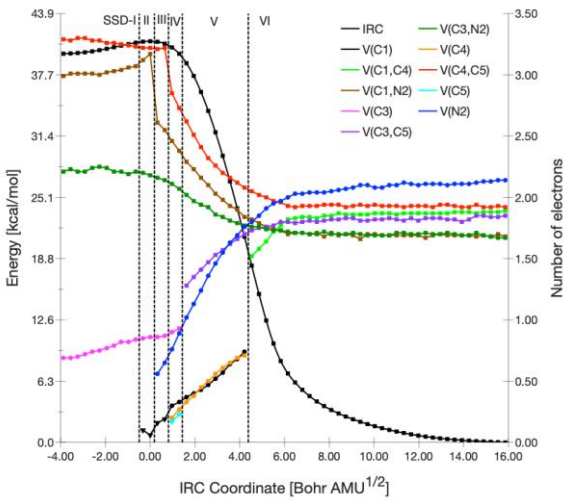

Fig. 11. IEFPCM(acetonitrile)/M06-2X/6–311+G(d,p) Population evolution (in e) of selected basins along the **TSN** reaction path of the 32CA reaction between **1** and **2**. The relative potential energy surface corresponds to the black dot curve.

http://dx.doi.org/10.29356/jmcs.v70i1.2572

J. Mex. Chem. Soc. **2026**, *70(1):e2572*
Regular Issue

ISSN-e 2594-0317

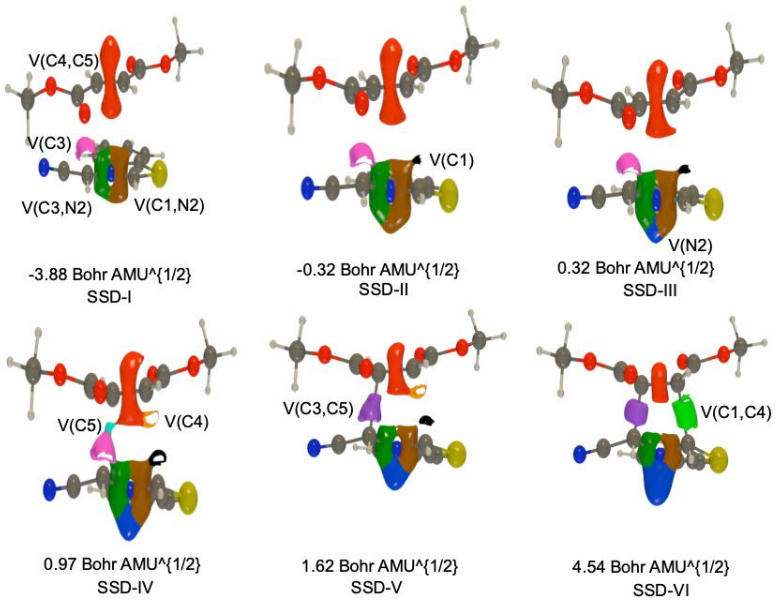

Fig. 12. IEFPCM(acetonitrile)/M06-2X/6–311+G(d,p) ELF (η = 0.72) snapshots of selected basins related to the bond forming process along the **TSN** reaction path.

Conclusions

In this comprehensive theoretical study, we investigated the reactivity of 1-(cyanomethyl)-2,3-dihydro-1H-benzothiazol-1-ium **1** toward dimethyl(Z)-2-butenedioate **2** in the framework of the MEDT using DFT calculations at the M06-2X/6-311+G(d,p) level in acetonitrile. Topological analysis of the ELF revealed that compound **1** behaves as a *carbenoid-type* TAC, with a highly reactive *carbenoid* C3 center, thereby categorizing this 32CA as a *cb-type* reaction. Reactivity indices from conceptual DFT indicated that TAC **1** is a moderate electrophile and a supernucleophile, while **2** acts as a strong electrophile and a poor nucleophile. These electronic features establish a significant electrophilicity-nucleophilicity interaction, supporting a polar character for this 32CA reaction. This electron density flow, directed from the TAC to the dipolarophile, aligns with a FEDF mechanism.

Due to the asymmetry of both reactants, the reaction proceeds through two competitive stereoisomeric pathways: *endo* and *exo*. Energetic analysis shows a slight kinetic and thermodynamic preference for the *endo* over the *exo* pathway. The TS-*endo* (**TSN**) is 0.27 kcal mol^{-1} lower in energy than TS-*exo* (**TSX**), with calculated populations confirming the dominance of **TSN** (60.12%). Moreover, both reaction pathways are strongly exothermic and irreversible, yielding stable *endo* and *exo* cycloadducts. The *endo* selectivity is further supported by RDG analysis, which demonstrated the presence of stronger NCIs in **TSN** compared to **TSX**. This finding aligns perfectly with the energetic and mechanistic data and supports the experimentally observed stereoselectivity.

BET analysis of the favored *endo* pathway identifies six SSDs characterized by successive electron density reorganizations. The mechanism is one-step but asynchronous, with early formation of the C3–C5 bond followed by the later formation of the C1–C4 bond. These insights are further corroborated by QTAIM and ELF analyses, reinforcing the detailed picture of bond formation and electron density shifts along the reaction path.

ISSN-e 2594-0317

Acknowledgements

M.C. is grateful to the University of Namur (UNamur) for granting him collaborator scientific status.

References

1. Padwa, A. I.; Pearson, W. H., in: *Synthesis Applications of 1,3-Dipolar Cycloaddition Chemistry*; Wiley, New York, **1984**.
2. Feuer, H. *Nitrile Oxides, Nitrones and Nitronates in Organic Synthesis: Novel Strategies in Synthesis*; John Wiley & Sons, **2008**.
3. Acharjee, N.; Mohammad-Salim, H. A.; Chakraborty, M. *Struct. Chem.* **2022**, *33*, 555–570. DOI: https://doi.org/10.21203/rs.3.rs-1122676/v1
4. Pérez, P.; Domingo, L. R.; Aurell, M. J.; Contreras, R. *Tetrahedron* **2003**, *59*, 3117–3125.
5. Domingo, L. R.; Saéz, J. A.; Zaragozá, R. J.; Arnó, M. *J. Org. Chem.* **2008**, *73*, 8791–8799.
6. Ríos-Gutiérrez, M.; Darù, A.; Tejero, T.; Domingo, L. R.; Merino, P. *Org. Biomol. Chem.* **2017**, *15*, 1618–1627.
7. Domingo, L. *Molecules* **2016**, *21*, 1319. DOI: https://doi.org/10.3390/molecules21101319
8. Xiao, Z.; Ding, T.; Mao, S.; Ning, X.; Kang, Y. *ChemInform* **2016**, *47*. DOI: https://doi.org/10.1002/chin.201641153
9. Wilson, A. K., in: *Frontiers in Computational Chemistry: Volume 5*; Bentham Science Publishers, **2020**; Vol. 5.
10. Ríos-Gutiérrez, M.; Domingo, L. R. *Eur. J. Org. Chem.* **2019**, *2019*, 267–282. DOI: https://doi.org/10.1002/ejoc.201800916
11. Parr, R. G.; Yang, W. *J. Am. Chem. Soc.* **1984**, *106*, 4049–4050. DOI: https://doi.org/10.1021/ja00326a036
12. Yang, W.; Mortier, W. J. *J. Am. Chem. Soc.* **1986**, *108*, 5708–5711. DOI: https://doi.org/10.1021/ja00279a008
13. Domingo, L. R.; Ríos-Gutiérrez, M. *Molecules.* **2017**, *22*, 750. DOI: https://doi.org/10.3390/molecules22050750
14. Wang, Y.; Wei, D.; Zhang, W.; Wang, Y.; Zhu, Y.; Jia, Y.; Tang, M. *Org. Biomol. Chem.* **2014**, *12*, 7503–7514
15. Nasri, L.; Ríos-Gutiérrez, M.; Nacereddine, A. K.; Djerourou, A.; Domingo, L. R. *Theor. Chem. Acc.* **2017**, *136*, 1–12
16. Domingo, L. R.; Chamorro, E.; Pérez, P. *Lett. Org. Chem.* **2010**, *7*, 432–439. DOI: https://doi.org/10.2174/157017810791824900
17. Domingo, L. R.; Ríos-Gutiérrez, M.; Pérez, P. *J. Org. Chem.* **2018**, *83*, 2182–2197. DOI: https://doi.org/10.1021/acs.joc.7b03093
18. Domingo, L. R.; Ríos-Gutiérrez, M.; Acharjee, N. *Molecules*. **2019**, *24*, 832. DOI: https://doi.org/10.3390/molecules24050832
19. Parr, R. G.; Yang, W. Annu. Rev. Phys. Chem. **1995**, *46*, 701–728. DOI: https://doi.org/10.1146/annurev.pc.46.100195.003413
20. Kohn, W.; Becke, A. D.; Parr, R. G. *J. Phys. Chem.* **1996**, *100*, 12974–12980. DOI: https://doi.org/10.1021/jp960669l
21. Ayers, P. W.; Parr, R. G. *J. Am. Chem. Soc.* **2000,** *122*, 2010–2018. DOI: https://doi.org/10.1021/ja9924039
22. De Proft, F.; Geerlings, P. *Chem. Rev.* **2001**, *101*, 1451–1464. DOI: https://doi.org/10.1021/cr9903205
23. Geerlings, P.; De Proft, F.; Langenaeker, W. *Chem. Rev.* **2003**, *103*, 1793–1874. DOI: https://doi.org/10.1021/cr990029p

ISSN-e 2594-0317

24. Domingo, L. R.; Ríos-Gutiérrez, M.; Pérez, P. *Molecules.* **2016**, *21*, 748. DOI: https://doi.org/10.3390/molecules21060748
25. Bader, R. F. W. *Acc. Chem. Res.* **1975**, *8*, 34–40. DOI: https://doi.org/10.1021/ar50085a005
26. Benallou, A.; Lakbaibi, Z.; El Alaoui El Abdallaoui, H. G. *Eur. Rev. Chem. Res.* **2018**, *5*. DOI: https://doi.org/10.13187/ercr.2018.2.42
27. Boutiddar, R.; Abbiche, K.; Mellaoui, M. D.; Imjjad, A.; Alahiane, M.; Ait Albrimi, Y.; Marakchi, K.; Mogren Al-Mogren, M.; El Hammadi, A.; Hochlaf, M. *J. Comput. Chem.* **2024**, *45*, 284–299. DOI: https://doi.org/10.1002/jcc.27235
28. Becke, A. D.; Edgecombe, K. E. *J. Chem. Phys.* **1990**, *92*, 5397–5403. DOI: https://doi.org/10.1063/1.458517
29. Johnson, E. R.; Keinan, S.; Mori-Sánchez, P.; Contreras-García, J.; Cohen, A. J.; Yang, W. *J. Am. Chem. Soc.* **2010**, *132*, 6498–6506. DOI: https://doi.org/10.1021/ja100936w
30. Domingo, L.; Acharjee, N., in: *Molecular Electron Density Theory: A New Theoretical Outlook on Organic Chemistry*; **2020**; 174–227. DOI: https://doi.org/10.2174/9789811457791120050007
31. Krokidis, X.; Noury, S.; Silvi, B. *J. Phys. Chem. A* **1997**, *101*, 7277–7282. DOI: https://doi.org/10.1021/jp9711508
32. Thom, R., in: *Structural Stability and Morphogenesis: An Outline of a General Theory of Models*; **1975**
33. Woodcock, E. R.; P. T. A. *Geometrical Study of Elementary Catastrophes*; Springer Berlin Heidelberg, **1974**
34. Gilmore, R., in: *Catastrophe Theory for Scientists and Engineers*; **1981**
35. Fukui, K. *Acc. Chem. Res.* **1981**, *14*, 363–368. DOI: https://doi.org/10.1021/ar00072a001
36. Adjieufack, A. I.; Ndassa, I. M.; Patouossa, I.; Mbadcam, J. K.; Safont, V. S.; Oliva, M.; Andrés, J. *Phys. Chem. Chem. Phys.* **2017**, *19*, 18288–18302. DOI: https://doi.org/10.1039/C7CP01016H
37. Adjieufack, A. I.; Liégeois, V.; Ndassa Mboumbouo, I.; Ketcha Mbadcam, J.; Champagne, B. *J. Phys. Chem. A* **2018**, *122*, 7472–7481. DOI: https://doi.org/10.1021/acs.jpca.8b06711
38. Kraus, G. A.; Nagy, J. O. *Tetrahedron* **1985**, *41*, 3537–3545. DOI: https://doi.org/10.1016/S0040-4020(01)96707-9
39. Zhao, Y.; Truhlar, D. G. *Theor. Chem. Acc.* **2008**, *120*, 215–241. DOI: https://doi.org/10.1007/s00214-007-0310-x
40. Mohammad-Salim, H.; de Julián-Ortiz, J. V.; Dahlous, K. A.; Islam, M. S.; Almutairi, T. M.; Benmetir, S. *Struct. Chem.* **2025**, *36*, 339–350. DOI: https://doi.org/10.1007/s11224-024-02373-7
41. Ouled Aitouna, A.; Mohammad-Salim, H.; Zeroual, A.; Syed, A.; Bahkali, A. H.; de Julián-Ortiz, J. V. *Comput. Theor. Chem.* **2023**, *1228*, 114283. DOI: https://doi.org/10.1016/j.comptc.2023.114283
42. Tomasi, J.; Mennucci, B.; Cammi, R. *Chem. Rev.* **2005**, *105*, 2999–3094. DOI: https://doi.org/10.1021/cr9904009
43. Domingo, L. R. *RSC Adv.* **2014**, *4*, 32415–32428. DOI: https://doi.org/10.1039/C4RA04280H
44. Reed, A. E.; Curtiss, L. A.; Weinhold, F. *Chem. Rev.* **1988**, *88*, 899–926. DOI: https://doi.org/10.1021/cr00088a005
45. Parr, R. G.; Yang, W., in: *Density-Functional Theory of Atoms and Molecules*; Oxford University Press, **1989**.
46. Parr, R. G.; Szentpály, L. v.; Liu, S. *J. Am. Chem. Soc.* **1999**, *121*, 1922–1924. DOI: https://doi.org/10.1021/ja983494x
47. Parr, R. G.; Pearson, R. G. *J. Am. Chem. Soc.* **1983**, *105*, 7512–7516. DOI: https://doi.org/10.1021/ja00364a005
48. Domingo, L. R.; Chamorro, E.; Pérez, P. *J. Org. Chem.* **2008**, *73*, 4615–4624. DOI: https://doi.org/10.1021/jo800572a
49. Reed, A. E.; Weinstock, R. B.; Weinhold, F. *J. Chem. Phys.* **1985**, *83*, 735–746. DOI: https://doi.org/10.1063/1.449486
50. Pérez, P.; Domingo, L. R.; Duque-Noreña, M.; Chamorro, E. *J. Mol. Struct. THEOCHEM.* **2009**, *895*, 86–91. DOI:https://doi.org/10.1016/j.theochem.2008.10.014
51. Chattaraj, P. K.; Duley, S.; Domingo, L. R. *Org. Biomol. Chem.* **2012**, *10*, 2855. DOI: https://doi.org/10.1039/c2ob06943a

ISSN-e 2594-0317

52. Frisch, M. J.; Trucks, G. W.; Schlegel, H. B.; Scuseria, G. E.; Robb, M. A.; Cheeseman, J. R.; Scalmani, G.; Barone, V.; Petersson, G. A.; Nakatsuji, H.; Li, X.; Caricato, M.; Marenich, A. V.; Bloino, J.; Janesko, B. G.; Gomperts, R.; Mennucci, B.; Hratchian, H. P. Gaussian 16, Revision B.01; **2016**. https://gaussian.com/gaussian16/
53. Contreras-García, J.; Johnson, E. R.; Keinan, S.; Chaudret, R.; Piquemal, J.-P.; Beratan, D. N.; Yang, W. *J. Chem. Theory Comput.* **2011**, *7*, 625–632. DOI: https://doi.org/10.1021/ct100641a
54. Lu, T.; Chen, F. *J. Comput. Chem.* **2012**, *33*, 580–592. DOI: https://doi.org/10.1002/jcc.22885
55. Noury, S.; Krokidis, X.; Fuster, F.; Silvi, B. *Comput. Chem.* **1999**, *23*, 597–604. DOI: https://doi.org/10.1016/S0097-8485(99)00039-X
56. https://www.unamur.be/fr/sciences/chimie/recherche/ucpts/lct/drawsuite/drawmol, accessed in September 2024.
57. https://www.unamur.be/fr/sciences/chimie/recherche/ucpts/lct/drawsuite/drawprofile, accessed in September 2024.
58. Chellegui, M.; Al-Mokhtar, R. M.; Salih, R. N.; Benhamed, L.; Benmetir, S.; Vicente de Julián-Ortiz, J.; Mohammad-Salim, H. A.; Ben Ahmed, A. *RSC Adv.* **2025**, *15*, 29666–29679. DOI: https://doi.org/10.1039/D5RA04992J
59. Chellegui, M.; Benhamed, L.; Salih, R. N.; Salhi, I.; Benmetir, S.; Ben Ahmed, A.; Mohammad-Salim, H. A.; de Julián-Ortiz, J. V. *RSC Adv.* **2025**, *15*, 32271–32283. DOI: https://doi.org/10.1039/D5RA04143K
60. Domingo, L. R.; Ríos-Gutiérrez, M.; Pérez, P. *Org. Biomol. Chem.* **2016**, *14*, 10427–10436. DOI: https://doi.org/10.1039/C6OB01989G
61. Domingo, L. R.; Ríos-Gutiérrez, M.; Pérez, P. *Tetrahedron.* **2016**, *72*, 1524–1532. DOI: https://doi.org/10.1016/j.tet.2016.01.061
62. Chellegui, M.; Champagne, B.; Trabelsi, M. *Theor. Chem. Acc.* **2022**, *141*, 21. DOI: https://doi.org/10.1007/s00214-022-02880-y
63. Chellegui, M.; Adjieufack, A. I.; Trabelsi, M.; Liégeois, V.; Champagne, B. *ChemPhysChem* **2025**, *26*. DOI: https://doi.org/10.1002/cphc.202400896
64. Chellegui, M.; Koudjina, S.; Salhi, I.; Benmetir, S.; Salih, R. N.; Mohammad-Salim, H. A.; Atohoun, G. Y. S.; de Julián-Ortiz, J. V. *Org. Biomol. Chem.* **2025**, *23*, 5016–5032. DOI: https://doi.org/10.1039/D5OB00529A
65. Chellegui, M.; Trabelsi, M.; Champagne, B.; Liégeois, V. *ACS Omega* **2025**, *10*, 833–847. DOI: https://doi.org/10.1021/acsomega.4c07888
66. Chellegui, M.; Benmetir, S.; Salih, R. N.; Mohammad-Salim, H. A.; de Julián-Ortiz, J. V.; Ben Ahmed, A. *New J. Chem.* **2025**, *49*, 7302–7313. DOI: https://doi.org/10.1039/D5NJ01058F
67. Chellegui, M.; Salhi, I.; Ben Ahmed, A.; Benmetir, S.; Salih, R. N.; Mohammad-Salim, H. A.; de Julián-Ortiz, J. V. *Struct. Chem.* **2025**. DOI: https://doi.org/10.1007/s11224-025-02520-8
68. Benmetir, S.; Chellegui, M.; Benhamed, L.; Al-Mokhtar, R. M.; Salih, R. N.; Algso, M. A.; de Julián-Ortiz, J. V.; Mohammad-Salim, H. A. *New J. Chem.* **2025**, *49*, 11191–11202. DOI: https://doi.org/10.1039/D5NJ01419K
69. Jaramillo, P.; Domingo, L. R.; Chamorro, E.; Pérez, P. *J. Mol. Struct. THEOCHEM*. **2008**, *865*, 68–72. DOI: https://doi.org/10.1016/j.theochem.2008.06.022
70. Domingo, L. R.; Ríos-Gutiérrez, M. *Sci. Radices* **2023**, *2*, 1–24. DOI: https://doi.org/10.58332/scirad2023v2i1a01
71. Aurell, M. J.; Domingo, L. R.; Pérez, P.; Contreras, R. *Tetrahedron* **2004**, *60*, 11503–11509. DOI: https://doi.org/10.1016/j.tet.2004.09.057
72. Domingo, L. R.; Pérez, P.; Sáez, J. A. *RSC Adv.* **2013**, *3*, 1486–1494. DOI: https://doi.org/10.1039/C2RA22886F
73. Domingo, L. R.; Ríos-Gutiérrez, M., in: *Conceptual Density Functional Theory*; Wiley, **2022**, 481–502. DOI: https://doi.org/10.1002/9783527829941.ch24
74. Boltzmann, L., in: *Ableitung Des Stefan'schen Gesetzes, Betreffend Die Abhangigkeit Der Warmestrahlung von Der Temperatur Aus Der Electromagnetischen Lichttheorie, von Ludwig Boltzmann in Graz*, **1877**

J. Mex. Chem. Soc. **2026**, *70(1):e2572*
Regular Issue

ISSN-e 2594-0317

75. Jasiński, R. *Chem. Heterocycl. Compd.* **2022**, *58*, 260–262. DOI: https://doi.org/10.1007/s10593-022-03081-y
76. Domingo, L. R.; Ríos-Gutiérrez, M. *Org. Biomol. Chem.* **2019**, *17*, 6478–6488. DOI: https://doi.org/10.1039/C9OB01031A
77. Boto, R. A.; Peccati, F.; Laplaza, R.; Quan, C.; Carbone, A.; Piquemal, J.-P.; Maday, Y.; Contreras-García, J. *J. Chem. Theory Comput.* **2020**, *16*, 4150–4158. DOI: https://doi.org/10.1021/acs.jctc.0c00063